Charge-carrier transport and recombination in heteroepitaxial CdTe

Darius Kuciauskas, Stuart Farrell, Pat Dippo, John Moseley, Helio Moutinho, Jian V. Li, A. M. Allende Motz, Ana Kanevce, Katherine Zaunbrecher, Timothy A. Gessert, Dean H. Levi, Wyatt K. Metzger, Eric Colegrove, and S. Sivananthan

Citation: Journal of Applied Physics **116**, 123108 (2014); doi: 10.1063/1.4896673
View online: http://dx.doi.org/10.1063/1.4896673
View Table of Contents: http://scitation.aip.org/content/aip/journal/jap/116/12?ver=pdfcov
Published by the AIP Publishing

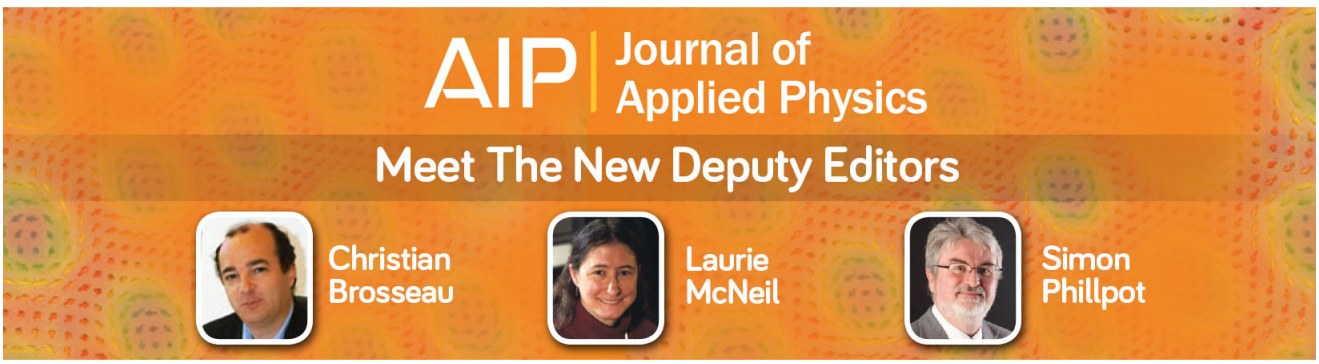

Charge-carrier transport and recombination in heteroepitaxial CdTe

Darius Kuciauskas,[1,a)] Stuart Farrell,[1] Pat Dippo,[1] John Moseley,[1] Helio Moutinho,[1] Jian V. Li,[1] A. M. Allende Motz,[1] Ana Kanevce,[1] Katherine Zaunbrecher,[1] Timothy A. Gessert,[1] Dean H. Levi,[1] Wyatt K. Metzger,[1] Eric Colegrove,[2] and S. Sivananthan[2]

[1]*National Renewable Energy Laboratory, 15013 Denver West Parkway, Golden, Colorado 80401-3305, USA*
[2]*Microphysics Laboratory, Physics Department, University of Illinois at Chicago, Chicago, Illinois 60612, USA*

(Received 6 June 2014; accepted 5 September 2014; published online 26 September 2014)

We analyze charge-carrier dynamics using time-resolved spectroscopy and varying epitaxial CdTe thickness in undoped heteroepitaxial CdTe/ZnTe/Si. By employing one-photon and nonlinear two-photon excitation, we assess surface, interface, and bulk recombination. Two-photon excitation with a focused laser beam enables characterization of recombination velocity at the buried epilayer/substrate interface, 17.5 μm from the sample surface. Measurements with a focused two-photon excitation beam also indicate a fast diffusion component, from which we estimate an electron mobility of 650 cm^2 $(Vs)^{-1}$ and diffusion coefficient D of 17 $cm^2\,s^{-1}$. We find limiting recombination at the epitaxial film surface (surface recombination velocity $S_{surface} = (2.8 \pm 0.3) \times 10^5\,cm\,s^{-1}$) and at the heteroepitaxial interface (interface recombination velocity $S_{interface} = (4.8 \pm 0.5) \times 10^5\,cm\,s^{-1}$). The results demonstrate that reducing surface and interface recombination velocity is critical for photovoltaic solar cells and electronic devices that employ epitaxial CdTe. © *2014 AIP Publishing LLC*. [http://dx.doi.org/10.1063/1.4896673]

I. INTRODUCTION

Efficiency of polycrystalline CdTe photovoltaic (PV) solar cells is increasing (current small-area cell record is 21% by First Solar),[1] but it is still much lower than the Shockley-Queisser limit. Efficiency losses are usually attributed to charge-carrier recombination, but the nature and location (bulk, grain boundary, surface/interface) of recombination centers are not clear.[2] Epitaxial materials provide a model system for the analysis of charge-carrier transport and recombination. Epilayers have also been used to produce PV devices. For example, relatively large open-circuit voltage was achieved with epitaxial $Cd_{1-x}Zn_xTe$.[3]

Heteroepitaxial CdTe/ZnTe/Si has been used for a long time as substrates for infrared (IR) detectors, but electronic and recombination properties of this system have not been studied in detail. Several groups have analyzed defect properties in heteroepitaxial CdTe using photoluminescence (PL) spectroscopy.[4–6] A key material property relevant for PV and other electronic devices is minority-carrier lifetime; however, we are aware of only one photoluminescence-based measurement of minority-carrier lifetime in epitaxial CdTe.[7] Carrier transport and diffusion in heteroepitaxial CdTe were also investigated by transient laser-induced grating spectroscopy.[8,9]

This paper reports detailed time-resolved photoluminescence (TRPL) studies in epitaxial CdTe grown on Si(211) substrates. We use one-photon and nonlinear two-photon excitation (1PE and 2PE, respectively). By using 1PE, we analyze surface recombination. In 2PE, generation occurs at the focus of the laser beam, which enables bulk characterization for samples with large surface recombination velocity. Combined 1PE and 2PE analysis to determine surface and bulk lifetimes has been applied to GaN,[10,11] ZnSe,[12] ZnO,[13] diamond,[14] and CdTe.[15–17] We extend this approach to characterize the buried epilayer/substrate interface. Characterization of buried interfaces with a focused 2PE laser beam does not require special sample preparation, and it avoids contamination or otherwise changing interface properties.

II. EXPERIMENTAL

A. Sample growth and characterization

To compare and contrast materials grown at different locations, heteroepitaxial CdTe was grown at the University of Illinois at Chicago (UIC) and at the National Renewable Energy Laboratory (NREL).[6,18] The substrate for molecular beam epitaxy (MBE) growth was undoped Si(211), and a thin (<50 nm) layer of ZnTe was employed to reduce lattice mismatch between CdTe and the Si substrate while also maintaining the (211) orientation.[6,18] Epilayer thicknesses were varied from 1.2 to 17.5 μm by altering deposition times and rates. Final thicknesses were determined by Fourier transform infrared spectroscopy (FTIR) thin-film interference fringes. The full width at half maximum (FWHM) of double-crystal rocking curve (DCRC) X-ray scans were used to evaluate the structural quality of all epilayers. For films thicker than 2 μm, *in situ* anneal cycles were performed to improve CdTe structural quality. Cathodoluminescence (CL) imaging was used to estimate dislocation density. Panchromatic CL was detected with a Ge photodiode. The contrast between the dark features and the bright areas was adjusted visually during the measurement with the contrast setting on the amplifier for the signal from the Ge diode. In this way, the brightest and darkest regions approximately

a)Darius.Kuciauskas@nrel.gov

correspond to the regions of highest and lowest CL intensity. Some samples were also characterized by electron backscattering diffraction (EBSD). Background doping of $(0.1–1) \times 10^{15}\,cm^{-3}$ was estimated from capacitance-voltage measurements. Theoretical arguments suggest p-type background doping because the dominant defect is V_{Cd}.[2,15] Near-bandgap PL emission spectra were measured with excitation at 632.8 nm. A closed-loop liquid helium cryostat was used for low-temperature PL measurements.

B. Time-resolved photoluminescence measurements

A regeneratively amplified Yb:KGW laser and optical parametric amplifier (Pharos/Orpheus, Light Conversion) were used for 1PE and 2PE TRPL measurements. Laser pulses with 300-fs width were fired at a rate of 1.1 MHz. A silicon avalanche photodiode (PDM, Micro Photon Devices) was used for time-correlated single-photon counting (with Picoharp 300E, PicoQuant). Interference filters (10-nm bandwidth, Thorlabs) were used in TRPL signal collection with 820-nm and 840-nm center wavelengths for 820 nm for 1PE and 2PE measurements, respectively. (The shift in the PL emission maximum with 2PE is attributed to reabsorption of the high-energy edge of the CdTe emission spectrum.[17]) A dichroic beamsplitter separated collinear excitation and PL signals. After deconvolution of the instrumental response function with Fluofit Pro 4.55 software (PicoQuant), we can resolve lifetimes down to 0.02 ns, which was sufficient for all samples in this study.

630-nm and 780-nm excitation was used in 1PE measurements. Based on CdTe absorption coefficients[19] at these wavelengths, the generation depth $(2.3/\alpha)$ was 0.5 μm at 630 nm and 1.0 μm at 780 nm.

1120-nm excitation was used in the 2PE measurements. The two-photon absorption coefficient β is much lower than the one-photon absorption coefficient α; therefore, carriers are generated nearly uniformly in the volume defined by the excitation beam size. Two different 2PE TRPL setups allowed measurements with relatively large and relatively small excitation volumes. The optical-fiber-based TRPL spectrometer employs a 1-m patch of multimode optical fiber QMMJ-IRVIS-100/140 (OZ Optics) and aspheric lens (New Focus 5721, NA 0.65), and it has an axial excitation spot diameter of $\sim$30 μm.[17] Characterization of the ultrafast pulse delivery for two-photon microscopy with similar QMMJ-IRVIS-50/125 optical fibers has been reported.[20] The 2PE TRPL measurement with the optical-fiber-based setup provides approximately uniform volume excitation throughout the depth of the epitaxial films with a thickness from 1.2 to 17.5 μm.

For high-spatial-resolution 2PE TRPL measurements, an A-Plan 40× NA0.65 microscope objective (Zeiss) with good near-IR transmittance was used. The laser beam was expanded using a telescope to slightly overfill the microscope aperture. The telescope magnification ratio was adjusted to obtain the best spatial resolution, and the sample was axially translated with a computer-controlled linear translation stage employing a motorized actuator Z812B (Thorlabs, minimal incremental movement of 0.05 μm, bidirectional repeatability $<$1.5 μm). An axial resolution of 5.5 ± 0.9 μm ($1/e^2$ width) for this setup was estimated from axial scans through the surface of the epitaxial CdTe sample. This axial resolution corresponds to 2.0 ± 0.3 μm lateral resolution, and this number was used in the data analysis.

For TRPL data analysis, the optical resolution needs to be compared with the diffusion length, L, for photogenerated carriers. For samples studied here, L is larger than 2 μm but less than 30 μm (see Sec. III D); therefore, we are able to investigate carrier transport from high-spatial-resolution TRPL measurements and recombination from low-spatial-resolution measurements.

III. RESULTS AND DISCUSSION

A. Low-temperature PL emission spectra

EBSD showed that CdTe epilayers have (211) orientation. The misalignment between the [211] direction and the surface normal was $\leq 5°$. Samples had good crystallinity indicated by high-quality Kikuchi patterns and by pole figures with minimum orientation spread. Grains or domains of different orientation were not observed.

Figure 1 shows PL emission spectra and corresponding CL images for three epitaxial samples. The excitation wavelength for PL was 632.8 nm, and 90% of incident photons were absorbed $2.3/\alpha = 0.5$ μm from the surface. Therefore, low-temperature near-bandgap PL emission spectra in Fig. 1 show evolution of the near-surface defect properties with epilayer thickness.

Low-temperature CdTe PL emission peaks can be divided into three groups, where emission is attributed to excitons, point defects, and extended defects.[21,22] For a 1.5-μm epilayer, PL emission is weaker (it is multiplied by 20× in Fig. 1), and exciton PL emission peaks are much smaller than the Y-defect emission with origin at 1.472 eV. Y-defect phonon replicas Y-LO (1.451 eV) and Y-2LO (1.430 eV) are also present. Y-defect emission has been attributed to

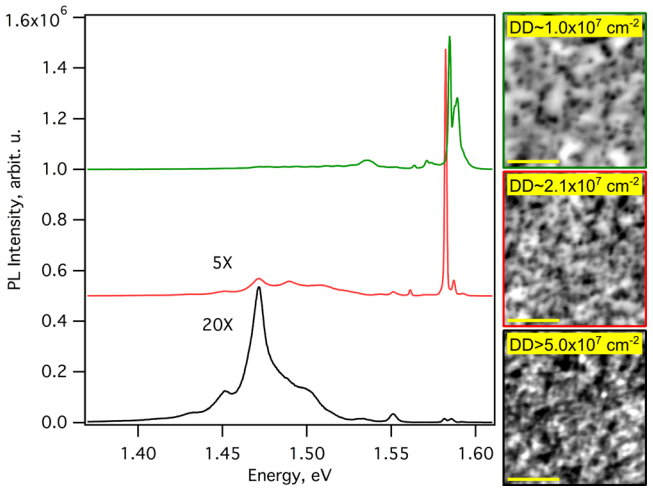

FIG. 1. Low-temperature (4.25 K) PL emission spectra for 1.5 μm (black), 7.2 μm (red), and 17.5 μm (green) heteroepitaxial CdTe. For clarity, the spectra are vertically offset; the first spectrum is multiplied by 20×, the second is multiplied by 5×. On the right, the corresponding CL images used to estimate the dislocation density (DD) are also shown. Scale bars in images are equal to 10 μm.

dislocations in epitaxial[4,5] and single-crystal CdTe.[23,24] Therefore, the PL emission spectrum for the 1.5-μm epilayer is dominated by dislocations. CL analysis shows that the surface dislocation density for this sample was $>5 \times 10^7\,cm^{-2}$.

For the epilayer with 7.2-μm thickness, both the Y-defect and exciton emission peaks are present. The PL emission is stronger than the 1.2-μm epilayer, but weaker than the 17.5-μm epilayer. The dislocation density from the CL analysis was $2.1 \times 10^7\,cm^{-2}$.

For the 17.5-μm epilayer, the dislocation density is further reduced to $1 \times 10^7\,cm^{-2}$. Here, exciton PL emission is dominant. Peaks at 1.594 (FX), 1.589 eV (DX), 1.587 eV (A_1X), and 1.585 eV (A_2X) are attributed to free excitons, donor-bound excitons, and acceptor-bound excitons, respectively.[21,22] Smaller-amplitude PL emission peaks are attributed to phonon replicas at 1.574 eV (FX-LO), 1.571 eV (A_1X-LO), and 1.564 eV (A_2X-LO).

Rujirawat *et al.* and Chen *et al.* have presented detailed structural analysis for heteroepitaxial CdTe/ZnTe/Si.[6,18] They found that large lattice mismatch introduces up to $10^{13}\,cm^{-2}$ misfit dislocations at the CdTe/ZnTe/Si heteroepitaxial interface region. Many of these dislocations are tangled and annihilate near the interface. Thereafter, threading dislocations propagate in the epitaxial layer and dislocation density decreases inversely with layer thickness. In their samples, dislocation density decreased to $\sim 3 \times 10^7\,cm^{-2}$ about 3 μm from the CdTe/ZnTe/Si interface region.[6,16] Similar to the study by Chen *et al.*,[6] we observe evolution of low-temperature PL emission spectra from Y-defect emission to exciton-dominated emission. Based on these data, it is clear that dislocations dominate PL emission for 1–2-μm-thick epilayers and are present to a lesser degree in thicker epilayers. In Sec. III D, we investigate their effect on charge-carrier dynamics.

At room temperature, PL emission (with maximum at 1.50 eV) is attributed to band-to-band recombination. Radiative efficiency is low, and nonradiative recombination largely determines overall recombination rate.

B. Recombination near the surface

TRPL decays for the 7.2-μm epilayer sample are shown in Fig. 2. 1PE decays can be described as two-exponential. Lifetimes measured with 630-nm excitation are $\tau_1 = 0.08$ ns ($A_1 = 0.87$ of total amplitude) and $\tau_2 = 0.44$ ns ($A_2 = 0.13$). The corresponding lifetimes for 780-nm excitation are $\tau_1 = 0.14$ ns ($A_1 = 0.80$) and $\tau_2 = 0.57$ ns ($A_2 = 0.20$). Average lifetimes calculated from the formula $\tau_{av} = A_1\tau_1 + A_2\tau_2$ are 0.13 and 0.23 ns for 630-nm and 780-nm excitation, respectively. 1PE TRPL decays were essentially the same when the excitation intensity was varied from $(0.5–2.0) \times 10^{13}$ photons cm^{-2} $pulse^{-1}$. In the case of surface recombination (see below), the excitation-intensity-independent lifetimes do not indicate trap saturation.

Biexponential 1PE TRPL decay shape is indicative of high surface recombination velocity.[11,17] After the laser pulse generates carriers in the sample, the time evolution of carrier concentration is governed by drift, diffusion, and recombination, and solutions to a diffusion equation for

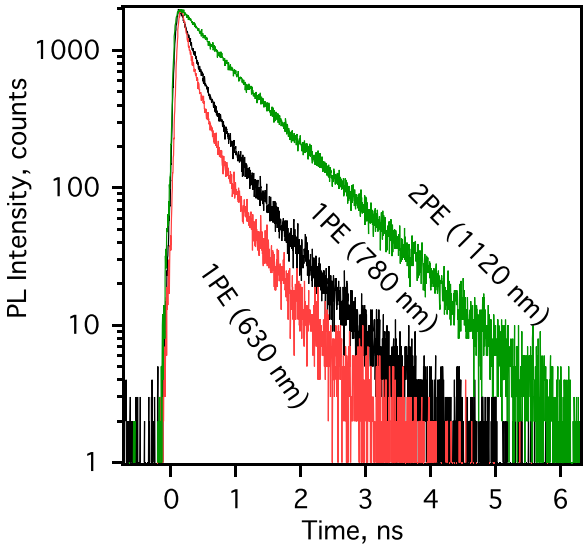

FIG. 2. 1PE and 2PE TRPL decays for 7.2 μm epilayer. 1PE excitation intensity was 1.0×10^{13} photons cm^{-2} $pulse^{-1}$; 2PE excitation intensity was 1.5×10^{16} photons cm^{-2} $pulse^{-1}$.

photogenerated carriers need to be considered in TRPL data analysis.[12,25,27–29] From solutions in the one-dimensional case, Ahrenkiel and Dashdorj have determined that the *initial* decay rate can be described as[25]

$$\frac{1}{\tau_1} = \frac{1}{\tau_B} + \alpha S, \tag{1}$$

where τ_B is bulk lifetime and S is surface recombination velocity. The first and second terms describe bulk and surface recombination rates, respectively. For high-quality single-crystal CdTe, $\alpha S \gg \tau_B^{-1}$ and S can be estimated from the experimental τ_1 value.[17] The diffusion lengths, L, corresponding to lifetimes τ_1 are very short: $L = 0.36$ μm (630-nm excitation) and $L = 0.49$ μm (780-nm excitation; diffusion coefficient $D = 17\,cm^2/s$ is estimated in Sec. III D). Both values are similar to absorption depths ($2.3/\alpha_{630nm}$ and $2.3/\alpha_{780nm}$); therefore, data suggest that the majority of the photogenerated carriers recombine close to the sample surface.

Wang *et al.* solved the diffusion equation for photogenerated carriers using a Fourier transform method and evaluated different non-exponential decay terms.[12] They found that the *dominant* lifetime can be described by the equation[12]

$$\frac{1}{\tau_{av}} = \frac{1}{\tau_B} + \frac{2\alpha^2 D}{1 + \sqrt{1 + 8\alpha^2 D/S^2}} \approx \frac{1}{\tau_B} + \frac{\alpha}{\sqrt{2}} S. \tag{2}$$

The simplified form can be used when $8\alpha^2 D^2/S^2 \gg 1$. Based on the value for D estimated in Sec. III D and the value for S estimated in the paragraph below, $8\alpha^2 D^2/S^2 \approx 60$ for 630-nm excitation and ≈ 30 for 780-nm excitation.

Surface recombination terms in Eqs. (1) and (2) differ by a factor of $\sqrt{2}$, which could be attributed to different approaches used in deriving the equations. Ahrenkiel and Dashdorj have estimated the *initial* decay rate, whereas Wang *et al.* have considered the *dominant* decay rate. Therefore, to estimate S, we use τ_1 in Eq. (1) and τ_{av} in Eq. (2). This yields $S = 2.8 \times 10^5\,cm\,s^{-1}$ (τ_1, 630 nm),

$S = 3.1 \times 10^5\,cm\,s^{-1}$ (τ_1, 780 nm), $S = 2.5 \times 10^5\,cm\,s^{-1}$ (τ_{av}, 630 nm), and $S = 2.7 \times 10^5\,cm\,s^{-1}$ (τ_{av}, 780 nm). The average value is $S = (2.8 \pm 0.3) \times 10^5\,cm\,s^{-1}$.

Very similar 1PE TRPL data were obtained for the other epitaxial samples. Within the error of measurement, 1PE TRPL decays were independent of the epilayer thickness. This suggests that S was similar for all samples in this series. However, the dislocation density strongly depends on epilayer thickness (Fig. 1). Hence, these data suggest that recombination occurs at other surface defects and not only at dislocations.

The surface recombination velocity for epitaxial CdTe is similar to that for other single-crystal or epitaxial semiconductors. For example, from PL-based analyses, $S = (1–3) \times 10^4\,cm\,s^{-1}$ for GaN,[11] $S = 5.8 \times 10^5\,cm\,s^{-1}$ for ZnSe,[12] $S = 1.0 \times 10^6\,cm\,s^{-1}$ for diamond,[14] and $S = 3 \times 10^6\,cm\,s^{-1}$ for GaAs.[26] Using nonlinear four-wave mixing measurements, it was determined that $S = 3 \times 10^6\,cm\,s^{-1}$ for CdTe,[9] $S = (0.2–5) \times 10^5\,cm\,s^{-1}$ for InP,[30] and $S = (0.3–3) \times 10^6\,cm\,s^{-1}$ for GaAs.[30]

C. Recombination for uniform generation with 2PE

The 1PE TRPL data described above provide estimates for S at the surface of the epitaxial sample, but the data are independent of the epitaxial layer thickness. To study bulk properties, we employ 2PE, where generation happens at the laser-beam focus. This section describes measurements where the generation volume axially spans the entire epitaxial layer. In Sec. III D, we describe measurements with 5.5-μm axial and 2.0-μm lateral spatial resolution, where generation volume can be selectively placed in the bulk.

The 2PE TRPL decay for the 7.5-μm sample (see Fig. 2) can be described as single-exponential with $\tau_{2PE} = 0.83$ ns, but these data alone do not establish if recombination has occurred in the absorber bulk or at interfaces. To learn about the dominant recombination pathway, in Figs. 3 and 4 we analyze 2PE TRPL decays and lifetimes for several heteroepitaxial samples. The inset in Fig. 4 shows the FWHM of X-ray

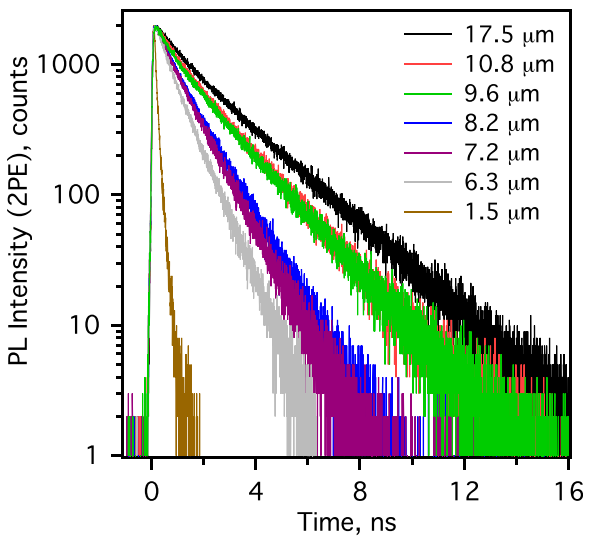

FIG. 3. 2PE TRPL decays for several heteroepitaxial samples. Epilayer thickness is indicated in the legend. Excitation intensity was 1.5×10^{16} photons cm^{-2} $pulse^{-1}$.

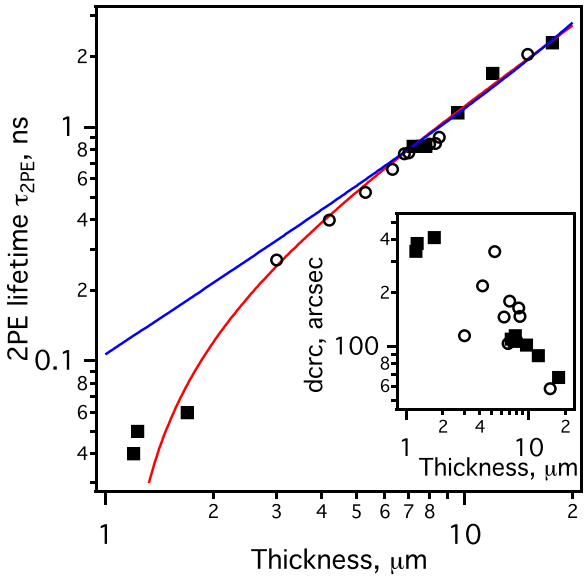

FIG. 4. Thickness dependence for τ_{2PE}. Squares—epilayers grown at UIC, circles—epilayers grown at NREL. Solid lines show fits to Eq. (3) when $a = 0$ (blue) and $a = 1.1 \pm 0.4\,\mu$m (red). The bulk recombination rate is $\tau_B^{-1} \approx 0.00 \pm 0.05\,ns^{-1}$ for both fits. The inset shows thickness-dependent XRD data.

data for the [422] square plane as a function of thickness for all 19 epilayers investigated in this study. Three samples with 1.2–1.5-μm thickness have substantially larger X-ray line widths. Dislocation density is the most significant factor that determines X-ray line width,[6,18] and all data (including PL emission spectra and CL images) are consistent with reduction of dislocation density for thicker epilayers.

All the 2PE decays in Fig. 3 can be described as single exponential. Furthermore, the lifetimes determined by 2PE TRPL were essentially the same when the excitation intensity was varied from $(0.8–3.0) \times 10^{16}$ photons cm^{-2} $pulse^{-1}$. The excitation-intensity-independent lifetimes suggest that the data correspond to low injection, and the exponential fitting model can be used in the data analysis. Figure 4 illustrates that the lifetimes show a strong correlation with the epilayer thickness. Figure 4 indicates data for samples grown at NREL, and separately at UIC. The overlap of the lifetime and XRD data indicates that the data are generic to the Si/ZnTe/CdTe system, rather than growth limitations on a particular piece of equipment.

The recombination rate for uniform generation was analyzed by Mayer *et al.*[27,28] They predict a single-exponential decay where the lifetime τ_{2PE} is given by

$$\frac{1}{\tau_{2PE}} = \frac{1}{\tau_B} + \frac{4\beta^2 D}{w^2} \approx \frac{1}{\tau_B} + \frac{2S_{2PE}}{w}. \quad (3)$$

The dimensionless coefficient β can be found from the equation $\beta \tan\beta = wS_{2PE}/2D$, which can only be solved for numerically. The effective thickness is expressed as $w = d–a$, where d is epilayer thickness determined by FTIR, and a is a correction factor that for our samples accounts for the surface/interface region width.[27,28] It is assumed that recombination is much faster at this interface layer than in the bulk. (This model assumes that surface and interface

recombination velocities are the same. Independent estimate of recombination velocity at the buried CdTe/ZnTe/Si interface region is given in Sec. III D, Fig. 6.) The simplified form of Eq. (3) is also widely used in the TRPL data analysis for double heterostructures.[29] The difference is that for double heterostructures, $a \approx 0$ and $w = d$.

This formula provides three plausible explanations for the 2PE lifetime data in Fig. 4. The first explanation is that interface recombination is dominant. The second explanation is that the defect density is inversely proportional to the thickness and drives bulk lifetime. The XRD FWHM is proportional to the defect density, and the XRD data in Fig. 4 are clearly inversely proportional to the epilayer thickness. This makes sense because as thickness increases, threading dislocations annihilate. The third possibility is that both mechanisms contribute.

We will assume at first that interface recombination is dominant. Figure 4 shows fits according to the simplified form of Eq. (3). The blue solid line corresponds to $w = d$ and does not fit well for samples with thickness in the 1.2–1.5-μm range. The red solid line corresponds to $a = 1.1 \pm 0.4\ \mu$m and gives a better fit. For samples with large lattice constant mismatch, such as CdTe/ZnTe/Si, the highly defective surface/interface region can extend deeply into the absorber.[6,18] This was evident in Fig. 1, where the 1.5-μm epilayer had only weak PL emission dominated by dislocations. Presumably, these dislocations have propagated from the CdTe/ZnTe/Si interface region. All 1.2–1.5-μm-thick samples had this feature, and we can expect that the value for a will be in this range.

These data also provide estimate for a recombination velocity near the buried interface. Both fits yield $S_{2PE} = (3.8 \pm 0.4) \times 10^5\,\mathrm{cm\,s^{-1}}$, which is similar to the estimate from the 1PE TRPL measurement (Fig. 2, $S = (2.8 \pm 0.3) \times 10^5\,\mathrm{cm\,s^{-1}}$). 2PE data were measured at lower injection than 1PE data; this might be one of the reasons for some difference in S values. It is also possible that $S_{interface}$ (at the CdTe/ZnTe/Si interface region) is larger than the $S_{surface}$ at CdTe surface. Therefore, we can estimate $S_{surface} = (2.8 \pm 0.3) \times 10^5\,\mathrm{cm\,s^{-1}}$ from 1PE measurements, and $S_{interface} = 2S_{2PE} - S_{surface} = (4.8 \pm 0.5) \times 10^5\,\mathrm{cm\,s^{-1}}$ from fits to data in Fig. 4.

Next, we consider bulk lifetime τ_B. If dislocations act as Shockley-Read-Hall (SRH) recombination centers, as the CL data indicates, then one expects that τ_B would be depth-dependent. Data in Fig. 4 do not allow us to distinguish unambiguously how bulk lifetime may contribute to the overall lifetime. However, the 1PE data do allow us to conclude that aggregate recombination is significantly limited by the surface. Interestingly, diffusion for photogenerated carriers must be sufficiently fast to allow transport to the surface over the distance of $\geq 8\ \mu$m (for carriers generated at the midpoint of the 17.5-μm epilayer). To learn more about transport, we performed initial Sentaurus Device simulations for TRPL decays.[33] Simulations indicate that for electron mobility of $650\,\mathrm{cm^2\,(Vs)^{-1}}$ (see Sec. III D below) bulk lifetime of ≥ 50 ns is required for carriers to diffuse over the distance of $\geq 8\ \mu$m. For shorter lifetimes, fewer carriers will reach the interface. An analytical model relating depth-dependent dislocation concentration to SRH lifetime is necessary for a more-detailed computational analysis. This work will be reported in the future.

To better characterize the heteroepitaxial interface and carrier transport in the bulk, Sec. III D describes direct microscopic measurements.

D. Recombination and transport for generation with a focused excitation beam

Figure 5 shows 2PE TRPL decays measured with a higher-resolution TRPL setup (for methods, see Sec. II B). The axial resolution of 5.5 μm (defined for $1/e^2$ width) is sufficient to resolve bulk and buried interface properties for the 17.5-μm epilayer. Unlike data for the same sample in Fig. 3, the decay in Fig. 5 is non-exponential. As shown in the inset, decays are largely independent of excitation intensity, which suggests that the non-exponential time dependence cannot be attributed to bimolecular recombination. (For 2PE, change in excitation intensity by 2× means an approximately 4× change in injection.) A simple model to analyze data in Fig. 5 is derived in the Appendix. Based on this model, we assume that the initial decay component of the decay is due to carrier diffusion from the excitation volume. Because 2PE decays are measured in low injection, the data reflect electron (minority-carrier) diffusion. A fit according to Eq. (A4) is shown as a solid red line and indicates an electron diffusion coefficient, where $D_e = 17.0 \pm 0.2\,\mathrm{cm^2\,s^{-1}}$. By using the Einstein relation, electron mobility could be estimated as $\mu_e = 650 \pm 10\,\mathrm{cm^2\,(Vs)^{-1}}$. This estimate is similar to the literature values for the electron mobility at room temperature in single-crystal CdTe ($600\,\mathrm{cm^2\,(Vs)^{-1}}$,[34] 800–$1000\,\mathrm{cm^2\,(Vs)^{-1}}$ (Ref. 35)). A diffusion coefficient of $29.5\,\mathrm{cm^2\,s^{-1}}$ for heteroepitaxial CdTe/ZnTe/GaAs was determined with transient grating spectroscopy and attributed to unipolar diffusion.[8] Because the CdTe epilayer was $<1\ \mu$m thick,[8]

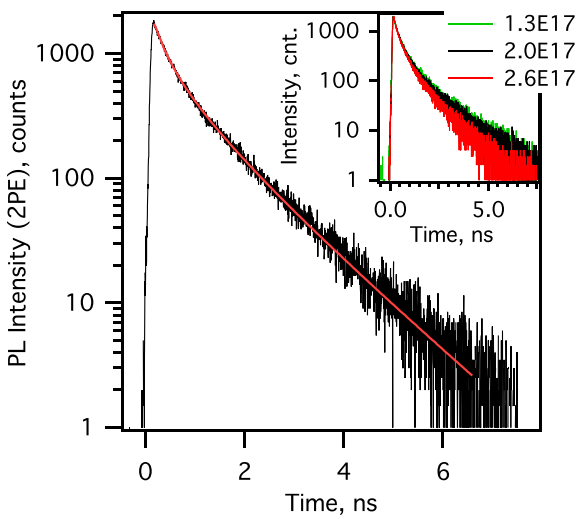

FIG. 5. 2PE TRPL decay measured with high-resolution setup when excitation beam was focused at the center of 17.5 μm thick epilayer. (These data correspond to the purple oval illustrated in the inset of Fig. 6.) Excitation intensity was 2×10^{17} photons $\mathrm{cm^{-2}}$ $\mathrm{pulse^{-1}}$. The solid red line shows the fit to Eq. (A4). Inset shows data measured with different excitation intensities indicated in the legend.

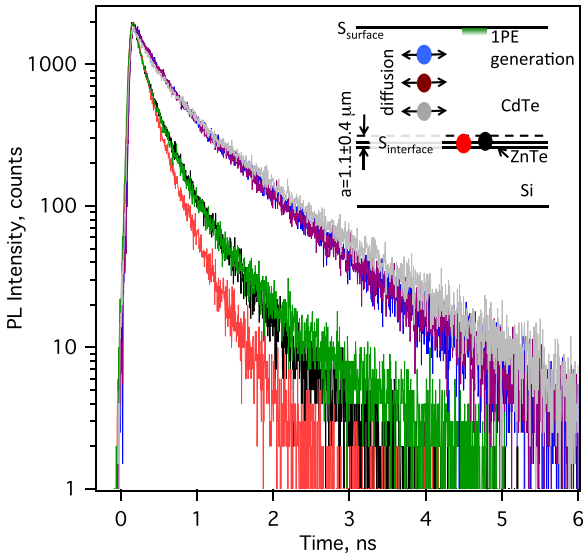

FIG. 6. TRPL decays measured at different axial depths as schematically indicated in the inset. Colors correspond to approximate 2PE generation locations shown as ovals. A heteroepitaxial interface with large $S_{interface}$ is indicated with a dashed line. Red and black decays correspond to generation close to the CdTe/ZnTe/Si interface region. Grey, purple, and blue decays were measured in the bulk when the sample was translated by 4 μm between measurements. 2PE excitation intensity was 2×10^{17} photons cm^{-2} pulse^{-1}. The green decay curve was measured with 1PE (630 nm, 1.5×10^{16} photons cm^{-2} pulse^{-1}) where generation was at the surface.

dislocation density probably was high (lattice-constant mismatch between CdTe and Si or GaAs is similar). Therefore, it appears that carrier mobility is not strongly affected by the high concentration of dislocations in heteroepitaxial CdTe.

The data in Fig. 5 describe diffusion on the 0–6-ns timescale, over which electrons diffuse $\sqrt{D_e t} \approx 3.2$ μm. This is sufficient to diffuse from the volume defined by the excitation beam size (estimated lateral excitation beam diameter was 2.0 μm). Because epilayers have depth-dependent defect concentration (Sec. III A), it is interesting to compare depth-dependent TRPL decays. These data are shown in Fig. 6, where the inset illustrates approximate generation locations in the epitaxial layer.

Figure 6 shows three decays (blue, purple, and grey) measured with excitation in the bulk of the 17.5-μm epilayer, where the sample was axially translated by 4 μm between the measurements. (Because of refraction at the air/epilayer interface, the optical path inside the sample is not the same as it would be in air,[16,36] and in Fig. 6 we reference the data to the external translation coordinate.) Three decays are essentially identical and can be fit with the same $D_e = 17.0 \pm 0.3$ cm^2 s^{-1} by using Eq. (A4). Therefore, depth-dependent dislocation density does not appear to change bulk transport dynamics over this range.

When 2PE is close to the heteroepitaxial Si/ZnTe/CdTe interface, recombination in Fig. 6 (red and black decays) is faster. It is unlikely that faster decays with excitation at the interface are due to faster carrier diffusion. More likely, lifetimes are shorter due to the large recombination velocity at the epilayer/substrate interface. For comparison, Fig. 6 also shows the 1PE TRPL decay from Fig. 2 (green), where generation was <0.5 μm from the surface. Data are similar, which suggests that recombination velocities at the epitaxial surface, $S_{surface}$, and heteroepitaxial interface, $S_{interface}$, are comparable. It appears that the region with large recombination velocity is wider at the heteroepitaxial interface than at the epilayer surface, because translation of the 2PE excitation spot by 1 μm at the heteroepitaxial interface (red and black decays) yielded similar fast decays. (In Fig. 4, the width of the recombination layer 1.1 ± 0.4 μm was estimated independently by fitting the data to Eq. (3).)

We applied exponential fitting to 2PE TRPL decays measured with excitation at the heteroepitaxial interface. Lifetimes of the initial decay components were $\tau_1 = 0.13 \pm 0.3$ ns and 0.08 ± 0.05 ns for black and red decays, respectively. To apply Eq. (1) and determine $S_{interface}$, we need to estimate the absorption coefficient. Many semiconductors have $\beta \approx 20$ cm GW^{-1},[37] and in this case α could be approximated as $\beta I_{peak} = 1.8 \times 10^3$ cm^{-1} (where $I_{peak} = 88$ GWcm^{-2} is the peak intensity for laser excitation with 2×10^{17} photons cm^{-2} pulse^{-1} and 0.3-ps pulse length). This yields $S_{interface} \approx (\beta I_{peak} \tau_1)^{-1} = (6 \pm 2) \times 10^5$ cm s^{-1} (uncertainty may be higher because β is not known). Within the uncertainty range, this value is in agreement with $S_{interface} = (4.8 \pm 0.5) \times 10^5$ cm s^{-1} derived from the independently measured data in Fig. 4.

IV. CONCLUSIONS

We have shown how to combine several TRPL analyses (1PE, 2PE, large-beam, and focused-beam measurements) to characterize semiconductor bulk and interface properties. This includes characterization of the buried interface without exposure of this interface to air, or otherwise changing its properties. Using this method, we have presented detailed analysis of recombination and transport dynamics in undoped heteroepitaxial CdTe/ZnTe/Si where the thickness of the CdTe epilayer ranged from 1.2 to 17.5 μm. The diffusion coefficient and mobility for minority carriers were estimated to be $D_e = 17.0 \pm 0.2$ cm^2 s^{-1} and $\mu_e = 650 \pm 10$ cm^2 (Vs)$^{-1}$, respectively. Despite a large and depth-dependent concentration of threading dislocations, we find that minority-carrier recombination predominantly occurs at the epitaxial surface and heteroepitaxial CdTe/ZnTe/Si interface region. From several independent measurements, recombination velocities were estimated as $S_{surface} = (2.8 \pm 0.3) \times 10^5$ cm s^{-1} and $S_{interface} = (4.8 \pm 0.5) \times 10^5$ cm s^{-1}. Recombination velocity $S_{surface}$ was independent of epilayer thickness, which implies that other defects, not dislocations, are dominant recombination centers at the CdTe surface. Further, data show that the region with large recombination velocity at the heteroepitaxial interface has an approximately 1.1 ± 0.4 μm width, but is much narrower at the epitaxial surface. Therefore, recombination at the heteroepitaxial interface is more similar to bulk recombination with large velocity due to a large concentration of defects, whereas recombination at the epitaxial surface largely occurs at the surface sites. Both recombination velocities are relatively high. Chemical treatments, similar to those described in the literature for single-crystal CdTe,[31,32] might be used to reduce recombination velocity at the epitaxial surface. A double heterostructure could also reduce recombination.[7] It might be more difficult to reduce large recombination velocity at the lattice-mismatched CdTe/ZnTe/Si interface region, which could present a limitation

for PV and other electronic devices that employ epitaxial CdTe grown on Si substrates.

ACKNOWLEDGMENTS

This work was supported by the U.S. Department of Energy under Contract No. DE-AC36-08-GO28308 with the National Renewable Energy Laboratory.

APPENDIX: ESTIMATING DIFFUSION COEFFICIENT FROM 2PE TRPL DATA WHEN CARRIER DIFFUSION LENGTH IS LARGER THAN THE EXCITATION BEAM DIAMETER

We assume an exponential decay for PL signal intensity, I(t)[29]

$$I(t) = I_0 e^{-\frac{t}{\tau_B}}, \tag{A1}$$

where I_0 is initial PL intensity, t is time, and τ_B is lifetime. Data in Fig. 3 are in good agreement with this model. Agreement is expected because, in this case, carriers are generated uniformly in a volume that spans the entire sample thickness, and carrier diffusion length L is smaller than the excitation beam diameter. Data are more complex when the measurement is carried out with a focused laser beam of radius u (Figs. 5 and 6). Here, we derive a simple model to explain these data by accounting for carrier diffusion.

In the collinear measurement geometry shown in Fig. 7, excitation (generation) and PL measurement volumes are assumed to be the same. Photogenerated carriers will diffuse from the initial excitation volume, which will decrease PL signal intensity. One-dimensional diffusion can be described by

$$I(x,t) = \frac{I(t)}{2\sqrt{\pi D t}} \exp\left(-\frac{x^2}{4Dt}\right), \tag{A2}$$

where D is diffusion coefficient and x is the coordinate. (This expression could be generalized for two-dimensional lateral diffusion by multiplying it by angle 2π. Because amplitude I_0 is an adjustable parameter in data analysis, the result would be the same.)

Excitation pulses and $I_{collected}$ follow the same optical path (but in opposite directions). Therefore, we assume that for carriers that diffused laterally from the excitation volume, photons emitted after radiative recombination will not be detected in the TRPL measurement. We neglect contributions to $I_{collected}$ due to PL scattered in the sample. For high-quality single-crystals, scattering is expected to be weak. We further simplify the problem by assuming that PL is only collected from the rectangle indicated by dashed lines in Fig. 7. Under these assumptions, the experimentally measured PL signal, $I_{collected}(t)$, will be

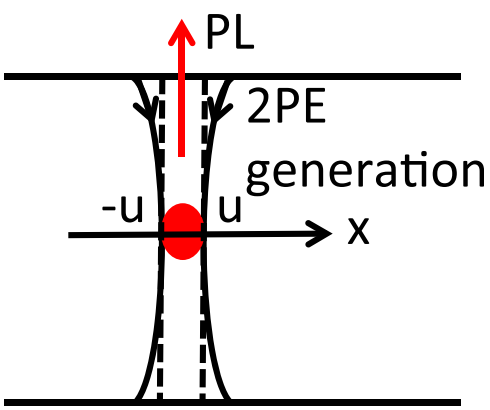

FIG. 7. Illustration of 2PE carrier generation with a focused laser beam (red oval). Lateral diffusion (coordinate x) from this volume reduces intensity of photoluminescence $I_{collected}$. Dashed lines indicate integration limits used to estimate $I_{collected}$.

$$I_{collected}(t) = \frac{I_0 e^{-\frac{t}{\tau_B}}}{2\sqrt{\pi D t}} \int_{-u}^{u} \exp\left(-\frac{x^2}{4Dt}\right) dx. \tag{A3}$$

After integration, time-dependent PL intensity is

$$I_{collected}(t) = I_0 erf\left(\frac{u}{2\sqrt{Dt}}\right) e^{-\frac{t}{\tau_B}}. \tag{A4}$$

Data analysis with Eq. (A4) is shown in Fig. 5. The error function primarily determines decay shape at early times, and fitting provides estimates for D. At low injection, the estimated diffusion coefficient is for minority carriers, D_e. At sufficiently long time delays after excitation, the error-function argument is small, and Eq. (A4) could be simplified as

$$I_{collected}(t) \approx \frac{I_0 u}{2\sqrt{Dt}} e^{-\frac{t}{\tau_B}}. \tag{A5}$$

Therefore, TRPL decays measured with a focused excitation beam (when $u \leq L$) will be non-exponential at all timescales. Data in Figs. 5 and 6 support this conclusion.

In summary, measurement with a focused laser beam allows estimating transport parameters (D and μ by using the Einstein relation), but τ_B is determined more reliably when the excitation spot diameter is larger than L. Combined 2PE TRPL measurements with large (Fig. 3) and focused (Figs. 5 and 6) laser beams provide for characterization of both transport (μ and D) and lifetime (τ_B).

This model makes several assumptions and simplifications. First, we did not consider excitation-beam refraction.[36] In principle, refraction effects could be reduced by using an oil-immersion objective or solid-immersion lens.[36] Second, the model does not account for reabsorption. Reabsorption will affect axial resolution for the measurement, but will have a smaller effect on lateral resolution. Third, the model does not consider diffraction, and Eq. (A4) could only be used when L is larger than the Abbe diffraction limit. Fourth, we assumed that a surface-induced electric field is not present; therefore, drift was not considered.

[1]See http://investor.firstsolar.com/releasedetail.cfm?ReleaseID=864426 for reported CdTe photovoltaic solar cell efficiency (accessed August 15, 2014).
[2]T. A. Gessert, S.-H. Wei, J. Ma, D. S. Albin, R. G. Dhere, J. N. Duenow, D. Kuciauskas, A. Kanevce, T. M. Barnes, J. M. Burst, W. L. Rance, M. O. Reese, and H. R. Moutinho, Sol. Energy Mater. Sol. Cells **119**, 149–155 (2013).
[3]M. Carmody, S. Mallick, J. Magetis, R. Kodama, T. Biegala, D. Xu, P. Bechmann, J. W. Garland, and S. Sivananthan, Appl. Phys. Lett. **96**, 153502 (2010).
[4]P. J. Dean, G. M. Williams, and G. Blackmore, J. Phys. D: Appl. Phys. **17**, 2291–2300 (1984).

[5]C. Onodera and T. Taguchi, J. Cryst. Growth **101**, 502–506 (1990).
[6]Y. Chen, S. Farrell, G. Brill, P. Wijewarnasuriya, and N. Dhar, J. Cryst. Growth **310**, 5303–5307 (2008).
[7]M. J. DiNezza, X.-H. Zhao, S. Liu, A. P. Kirk, and Y.-H. Zhang, Appl. Phys. Lett. **103**, 193901 (2013).
[8]V. Mizeikis, K. Jarasiunas, N. Lovergine, and P. Prete, J. Cryst. Growth **214/215**, 234–239 (2000).
[9]K. Jarasiunas, E. Gaubas, R. Aleksiejunas, M. Sudzius, V. Gudelis, T. Malinauskas, P. Prete, A. M. Mansini, and N. Lovergine, Phys. Status Solidi A **195**, 238–242 (2003).
[10]S. Juršėnas, S. Miasojedovas, A. Žukauskas, B. Lucznik, I. Grzegory, and T. Suski, Appl. Phys. Lett. **89**, 172119 (2006).
[11]P. Ščajev, K. Jarašiūnas, S. Okur, U. Oüzgür, and H. Morkoç, J. Appl. Phys. **111**, 023702 (2012).
[12]H. Wang, K. S. Wong, B. A. Foreman, Z. Y. Yang, and G. K. L. Wong, J. Appl. Phys. **83**, 4773 (1998).
[13]S. Yamamoto, H. Sakuma, and T. Mishina, Jpn. J. Appl. Phys., Part 1 **49**, 121102 (2010).
[14]M. Kozák, F. Trojánek, and P. Malý, Opt. Lett. **37**, 2049 (2012).
[15]J. Ma, D. Kuciauskas, D. Albin, R. Bhattacharya, M. Reese, T. Barnes, J. V. Li, T. Gessert, and S. Wei, Phys. Rev. Lett. **111**, 067402 (2013).
[16]E. S. Barnard, E. T. Hoke, S. T. Connor, J. R. Groves, T. Kuykendall, Z. Yan, E. C. Samulon, E. D. Bourret-Courchesne, S. Aloni, P. J. Schuck, C. H. Peters, and B. E. Hardin, Sci. Rep. **3**, 2098 (2013).
[17]D. Kuciauskas, A. Kanevce, J. M. Burst, J. N. Duenow, R. Dhere, D. S. Albin, D. H. Levi, and R. K. Ahrenkiel, IEEE J. Photovoltaics **3**, 1319–1324 (2013).
[18]S. Rujirawat, L. A. Almeida, Y. P. Chen, S. Sivananthan, and D. J. Smith, Appl. Phys. Lett. **71**, 1810–1812 (1997).
[19]D. E. Aspnes and H. Arwin, J. Vac. Sci. Technol., A **2**, 1309–1315 (1984).
[20]D. Kim, H. Choi, S. Yazdanafar, and P. T. C. So, Microsc. Res. Tech. **71**, 887–896 (2008).
[21]C. Kraft, H. Metzner, M. Haüdrich, U. Reisloühner, P. Schley, G. Gobsch, and R. Goldhahn, J. Appl. Phys. **108**, 124503 (2010).
[22]D. Albin, D. Kuciauskas, J. Ma, W. Metzger, J. Burst, H. Moutinho, and P. Dippo, Appl. Phys. Lett. **104**, 092109 (2014).
[23]S. Hildebrandt, H. Uniewski, J. Schreiber, and H. S. Leipner, J. Phys. III **7**, 1505–1514 (1997).
[24]S. Seto, A. Tanaka, F. Takeda, and K. Matsuura, J. Cryst. Growth **138**, 346–351 (1994).
[25]R. K. Ahrenkiel and J. Dashdorj, J. Vac. Sci. Technol., B **22**, 2063–2067 (2004).
[26]F. Cadiz, D. Paget, A. C. H. Rowe, V. L. Berkovits, V. P. Ulin, S. Arscott, and E. Peytavit, J. Appl. Phys. **114**, 103711 (2013).
[27]G. Mayer, B. E. Maile, R. Germann, and A. Forchel, Superlattices Microstruct. **5**, 579–582 (1989).
[28]G. Mayer, B. E. Maile, R. Germann, A. Forchel, P. Grambow, and H. P. Meier, Appl. Phys. Lett. **56**, 2016 (1990).
[29]R. K. Ahrenkiel, "Minority carrier lifetime in III-V semiconductors," Semicond. Semimet. **39**, 39–150 (1993).
[30]C. A. Hoffman, H. J. Gerritsen, and A. V. Nurmikko, J. Appl. Phys. **51**, 1603 (1980).
[31]C. K. Kang, S. U. Yuldashev, J. H. Leem, Y. S. Ryu, J. K. Hyun, H. S. Jung, H. J. Kim, T. W. Kang, H. I. Lee, Y. D. Woo, and T. W. Kim, J. Appl. Phys. **88**, 2013 (2000).
[32]R. Cohen, V. Lyahovitskaya, E. Poles, A. Liu, and Y. Rosenwaks, Appl. Phys. Lett. **73**, 1400–1402 (1998).
[33]A. Kanevce, D. H. Levi, and D. Kuciauskas, "The role of drift, diffusion, and recombination in time-resolved photoluminescence of CdTe solar cells determined through numerical simulation," Prog. Photovoltaics (published online).
[34]J. L. Pankove, *Optical Processes in Semiconductors* (Dover Publications, 1971), p. 422.
[35]Collaboration: Authors and editors of the volumes III/17B-22A-41B, *Cadmium Telluride (CdTe) Electrical and Thermal Transport, Carrier Mobilities*, edited by O. Madelung, U. Rössler, and M. Schulz, Springer Materials—The Landolt-Börnstein Database (Springer, 2008).
[36]N. J. Everall, Appl. Spectrosc. **54**, 773–782 (2000).
[37]V. Nathan, A. H. Guenther, and S. S. Mitra, J. Opt. Soc. Am. B **2**, 294–316 (1985).